Acta Crystallographica Section D
Biological Crystallography
ISSN 0907-4449

Catalysis product captured in lumazine synthase from the fungal pathogen *Candida glabrata*

Madhu Shankar,[a,b] Sigurd M. Wilbanks,[c] Yoshio Nakatani,[c] Brian C. Monk[b] and Joel D. A. Tyndall[a]*

[a]School of Pharmacy, University of Otago, PO Box 56, Dunedin 9054, New Zealand, [b]Sir John Walsh Research Institute, University of Otago, PO Box 647, Dunedin 9054, New Zealand, and [c]Department of Biochemistry, University of Otago, PO Box 56, Dunedin 9054, New Zealand

Correspondence e-mail: joel.tyndall@otago.ac.nz

Received 6 March 2013
Accepted 23 April 2013

PDB Reference: lumazine synthase, 4kq6

Candida glabrata has emerged as an important fungal pathogen with intrinsic resistance to azole drugs. The limited efficacy of and resistance to existing antifungals is driving the need to identify new drug targets. The enzyme 6,7-dimethyl-8-(D-ribityl)lumazine synthase is part of the riboflavin-biosynthesis pathway essential to fungi and bacteria and is a potential drug target for the development of broad-spectrum antifungal drugs. The X-ray crystal structure of recombinant lumazine synthase from *C. glabrata* was obtained at 2.24 Å resolution and revealed a dimer of homopentamers, with one in five subunits containing a product molecule from the catalytic reaction.

1. Introduction

There has been a steady rise in the number of fungal species recognized as causing life-threatening infections (Rajeshkumar & Sundararaman, 2012; Messer *et al.*, 2006; Pfaller & Diekema, 2010; Pfaller *et al.*, 2006). The most prominent of the fungal pathogens that affect the human host are *Candida albicans*, *Aspergillus fumigatus*, *Pneumocystis pneumoniae*, *C. glabrata*, *C. parapsilosis*, *C. krusei* and *Cryptococcus neoformans* (Pfaller & Diekema, 2007). Despite this formidable list of opportunistic fungi, *Candida* species remain the most prominent cause of opportunistic mycoses, with *C. albicans* causing approximately 50% of fungal infections (Messer *et al.*, 2006). In the past decade *C. glabrata* has emerged as a more important pathogen, particularly owing to infections caused by innately fluconazole-resistant members of this species. *C. glabrata* is now a serious health risk to cancer patients, AIDS patients, diabetics, newborns and the elderly (Kusne & Blair, 2006). *C. glabrata* accounted for 17% of fungaemias during an eight-year study in medical centres in the United States (Malani *et al.*, 2005). In Australia between 2001 and 2004, *C. glabrata* was found to be the third most common species causing candidaemia (Chen *et al.*, 2006). It was responsible for 15% of candidaemias overall and was found to be the causative agent in 53.3% of episodes of fungal infection in patients of >65 years of age, an alarming trend in an ageing population (Chen *et al.*, 2006).

All organisms require riboflavin (vitamin B_2). It is a precursor of the cofactors flavin mononucleotide (FMN) or flavin adenine dinucleotide (FAD) present in flavoproteins (Massey, 2000). The riboflavin-biosynthetic pathway is an attractive drug target in pathogens because fungi, plants and bacteria lack uptake pathways and synthesize riboflavin, whereas animals obtain the vitamin from dietary sources. The biosynthesis of riboflavin has been extensively researched (Fischer & Bacher, 2008, 2011; Kis *et al.*, 1995). The enzyme

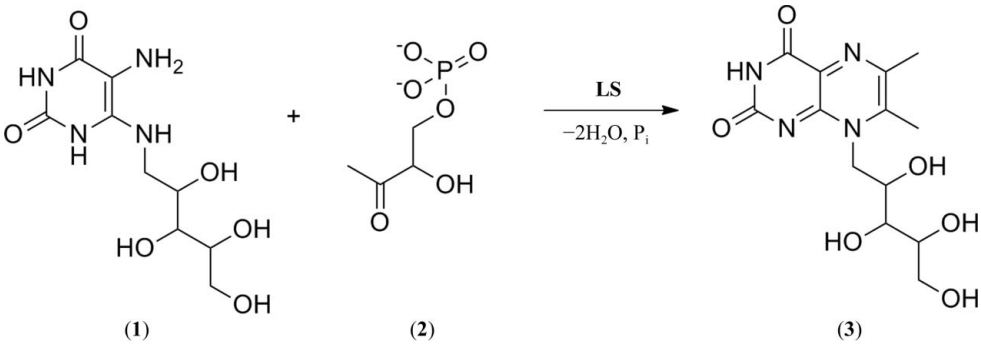

Figure 1
The penultimate step in riboflavin biosynthesis catalysed by lumazine synthase (LS). Condensation of 5-amino-6-ribitylamino-2,4-(1*H*,3*H*)pyrimidinedione (**1**) with 3,4-dihydroxy-2-butanone-4-phosphate (**2**) produces 6,7-dimethyl-8-(D-ribityl)lumazine (**3**).

6,7-dimethyl-8-(D-ribityl)lumazine synthase (EC 2.5.1.78) or lumazine synthase (LS) catalyses the penultimate step in the synthesis of riboflavin *via* the condensation of 5-amino-6-ribitylamino-2,4-(1*H*,3*H*)pyrimidinedione with 3,4-dihydroxy-2-butanone-4-phosphate (DHBP) to produce 6,7-dimethyl-8-(D-ribityl)lumazine (Fig. 1), which then acts as a substrate for riboflavin synthase.

Structures have been determined of LS from several pathogenic organisms, including *Mycobacterium tuberculosis* (Morgunova *et al.*, 2005), *Bacillus anthracis* (Morgunova *et al.*, 2010), *Salmonella enterica* subsp. (Kumar *et al.*, 2011) and *C. albicans* (Morgunova *et al.*, 2007), as well as from the model yeast *Saccharomyces cerevisiae* (Meining *et al.*, 2000). The protein exists in several different multimeric forms [pentameric, decameric (Klinke *et al.*, 2005) or icosahedral (Zhang *et al.*, 2001)]. The minimal assembly is a pentamer containing five identical active sites. In this study, we present the 2.24 Å resolution X-ray crystal structure of *C. glabrata* LS fortuitously complexed with the product of catalysis, 6,7-dimethyl-8-(D-ribityl)lumazine.

2. Materials and methods

2.1. Cloning, expression and purification

The *RIB4* gene encoding lumazine synthase (UniProt Q6FXA8) was amplified from *C. glabrata* genomic DNA by PCR using the oligonucleotide primers Cg*RIB4*2F (5′-TA **CCA TGG** CAG TTA AGG GAT TGG GTC AAT T-3′) and Cg*RIB4*2R (5′-AT **AGA TCT** AGC ATT GGC ACC GAA CTT-3′) supplied by Invitrogen. The amplified PCR product was digested with the restriction enzymes *Bam*HI and *Sal*I (New England Biolabs; recognition sequences are shown in bold in the primer sequences) and was ligated into the pQE30 expression vector (Qiagen). The resultant plasmid, RIB4pQE30, was transformed into the *Escherichia coli* host M15[pREP4] (Qiagen) carrying the pREP4 plasmid which overexpresses the *lac* repressor. The correct gene sequence for the recombinant *C. glabrata* RIB4 construct was confirmed by DNA-sequence analysis.

The recombinant *E. coli* M15[pREP4] strain was grown in lysogeny broth containing ampicillin (100 µg ml^{-1}) and kanamycin (25 µg ml^{-1}). The culture was incubated at 310 K at 200 rev min^{-1} until the $OD_{600\ nm}$ reached 0.6, at which point isopropyl β-D-1-thiogalactopyranoside (IPTG) was added to a final concentration of 0.5 m*M* and the culture was incubated overnight at 293 K and 200 rev min^{-1}. The cells were harvested by centrifugation at 3200*g* for 10 min at 277 K, resuspended in 3 ml homogenization buffer (50 m*M* NaH_2PO_4 pH 8, 300 m*M* NaCl, 10 m*M* imidazole, 0.5 m*M* PMSF) and stored at 253 K until further use. Frozen cells were thawed, lysozyme (1 mg ml^{-1}) was added and the solution was incubated for 30 min on ice. The cells were lysed on ice by sonication (Branson Digital sonifier; 10 mm horn, 17% power) for 2 min with alternating 10 s pulses and pauses. The lysate was clarified by centrifugation at 12 000*g* for 30 min at 277 K.

The clarified lysate was fractionated using Ni–NTA agarose affinity resin (Qiagen) equilibrated with lysis buffer (as for the homogenization buffer but without PMSF). 1 ml 50% Ni–NTA agarose was added to 4 ml of the lysate and mixed gently on a rotary shaker at 200 rev min^{-1} for 60 min at 277 K. The mixture was loaded into a polypropylene column, the column flowthrough was collected and the Ni–NTA resin was washed twice with 4 ml lysis buffer. The bound protein was eluted using the same buffer containing a step series of imidazole concentrations between 10 and 300 m*M*. SDS–PAGE analysis showed a dominant species of the molecular weight expected for LS (19 500 Da) which eluted at 200 m*M* imidazole.

The affinity-purified protein was separated by size-exclusion chromatography (SEC) using a Superdex 200 10/300 column (GE Healthcare Life Sciences, UK) equilibrated with 100 m*M* potassium phosphate buffer pH 7 (a mixture of K_2HPO_4 and KH_2PO_4 adjusted with KOH where necessary), 300 m*M* NaCl at a flow rate of 0.5 ml min^{-1}. The fractions containing purified LS were concentrated using an Amicon Ultra-4 centrifugal filter device with a 30 kDa molecular-weight cutoff (Millipore). The primary sequence, the intact mass and the presence of product were confirmed by mass spectrometry using an ABI 4800 MALDI tandem time-of-flight mass spectrometer.

2.2. Crystallization

C. glabrata LS was crystallized using the hanging-drop vapour-diffusion method. Initial crystallization trials were carried out using the JCSG-*plus* screen (Molecular Dimensions), crystal screens from Hampton Research and a custom ammonium sulfate screen. Each hanging drop consisted of 200 nl protein (8.4 mg ml^{-1}) in 100 m*M* potassium phosphate buffer pH 7.5, 150 m*M* NaCl and 200 nl reservoir solution and

Table 1
Data-collection and refinement statistics.

Values in parentheses are for the highest resolution shell.

PDB code	4kq6
Space group	$P2_12_12_1$
Unit-cell parameters (Å)	a = 84.75, b = 84.84, c = 310.20
Unique reflections	101325
Resolution (Å)	47.43–2.24 (2.36–2.24)
Multiplicity	5.31 (2.13)
Completeness (%)	97.4 (88.6)
$\langle I/\sigma(I)\rangle$	15.0 (5.8)
$R_{\rm merge}$†	0.083 (0.280)
Refinement	
$R_{\rm cryst}$‡	0.200 (0.53)
$R_{\rm free}$§	0.252 (0.53)
No. of atoms in model	
Protein	12184
Ligand (catalytic product)	46
Sulfate molecules	24
Glycerol molecules	5
Water molecules	933
Deviation from ideal bond lengths (Å)	0.024
Deviation from ideal bond angles (°)	1.925
Average B factor (Å^2)	20.62
Average B factor, product (Å^2)	24.97
Average B factor, sulfate (Å^2)	49.13
Ramachandran analysis, residues in (%)	
Preferred regions	97.0
Allowed regions	2.4
Disallowed regions	0.6

† $R_{\rm merge} = \sum_{hkl}\sum_i |I_i(hkl) - \langle I(hkl)\rangle|/\sum_{hkl}\sum_i I_i(hkl)$. ‡ $R_{\rm cryst} = \sum_{hkl}||F_{\rm obs}| - |F_{\rm calc}||/\sum_{hkl}|F_{\rm obs}|$ computed over a working set composed of 95% of the data. § $R_{\rm free} = \sum_{hkl}||F_{\rm obs}| - |F_{\rm calc}||/\sum_{hkl}|F_{\rm obs}|$ computed over a test set composed of 5% of the data.

was equilibrated against 100 µl reservoir solution in 96-well plates at 291 K. The crystal for data collection was prepared using a reservoir solution consisting of 1.6 *M* ammonium sulfate, 100 m*M* sodium acetate pH 5.5, 100 m*M* sodium chloride. Crystals grew after one week and were allowed to grow for a further two weeks until their major dimensions exceeded 200 µm. The resulting crystal was soaked in reservoir solution containing 20% glycerol as a cryoprotectant for several minutes and was flash-cooled in liquid nitrogen prior to data collection.

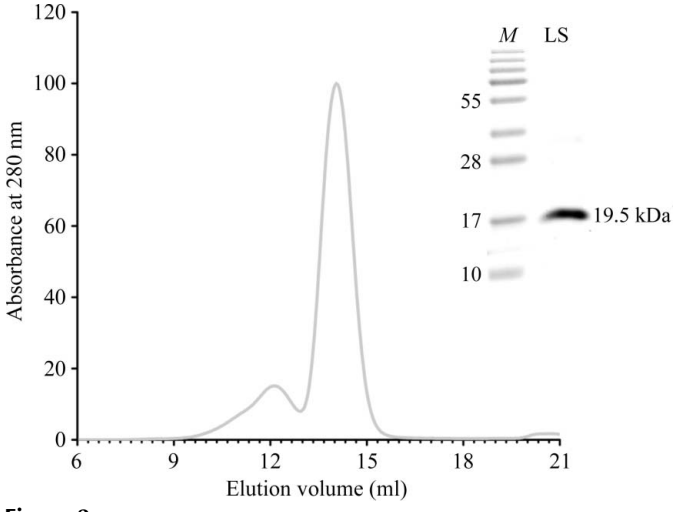

Figure 2
Size-exclusion chromatogram (Superdex 200) of LS showing a small decamer peak (∼12 ml) eluting prior to the pentameric form of LS (main peak, ∼14 ml). The inset shows an SDS–PAGE gel of SEC-purified LS. Lane *M*, molecular-weight standards; sizes are indicated on the left in kDa.

2.3. Data collection and processing

Data were collected on the MX2 beamline at the Australian synchrotron using an ADSC Quantum 315 detector. A complete data set was obtained at a wavelength of 0.954 Å with an oscillation range of 1.0°. The diffraction data were processed with *iMosflm* (Battye *et al.*, 2011) and *SCALA* (Evans, 2006). For phasing, molecular replacement was implemented using *Phaser* (using PDB entry 1ejb as a search model; Meining *et al.*, 2000). Modelling and refinement of the structure was carried out using *Coot* (Emsley *et al.*, 2010) and *REFMAC* (Murshudov *et al.*, 2011) from the *CCP*4 suite (Winn *et al.*, 2011). Water molecules were added where at least one possible hydrogen bond existed (2.5–3.3 Å). The product and other solvent molecules were subsequently modelled into appropriate density. The occupancy of the product was refined at 50%, except for the glycerol moiety of the ribityl chain, which was refined at 100%. Medium noncrystallographic symmetry restraints were applied to each LS monomer during refinement.

2.4. Fluorescence spectroscopy

Fluorescence spectroscopy was used to confirm the presence of the product 6,7-dimethyl-8-(D-ribityl)lumazine in the LS sample. The fluorescence excitation and emission spectra of LS protein (48 µ*M*) and commercial riboflavin (10 µ*M*) were obtained from 200 to 600 nm in 50 m*M* phosphate buffer pH 7.0 using a Hitachi F-7000 (USA) spectrofluorometer equipped with a 1 cm cuvette.

3. Results and discussion

3.1. Protein purification

The full-length LS was expressed in *E. coli* and was purified to >95% homogeneity by Ni–NTA affinity chromatography and SEC (Fig. 2). LS eluted from SEC predominantly as a pentamer with some decamer present. MALDI–TOF mass spectrometry determined that the mass of the protein complex was 97 770 Da. This confirmed that the LS was present as a pentamer (predicted mass of 19 548.2 Da for a monomer including the hexahistidine tag).

3.2. Lumazine synthase structure

A pentameric sample of LS was used for crystallization. Data-collection parameters and refinement statistics are listed in Table 1. Refinement was carried out with the use of tenfold noncrystallographic symmetry (medium restraints). The LS model was refined to an $R_{\rm cryst}$ of 0.200 and an $R_{\rm free}$ of 0.252. The final model has been deposited as PDB entry 4kq6.

Molecular replacement using *S. cerevisiae* LS (Meining *et al.*, 2000) revealed two pentamers in the asymmetric unit (Fig. 3). *PISA* (Krissinel & Henrick, 2007) predicted a pentamer to be the most probable assembly. LS has previously

been observed as a decamer from *Brucella* spp. (Klinke *et al.*, 2005); however, the current structure differs as the pentamer interface is formed *via* a tail-to-tail interaction (Fig. 3*b*). Contact between pentamers occurs *via* water-mediated hydrogen bonds between the main-chain carbonyl O atoms of Ala76 and Lys77 of each adjacent monomer (Fig. 4). This pentamer interface and these hydrogen-bonded contacts are also seen between the homopentamer and a symmetry-related molecule of LS from *S. cerevisiae* (Meining *et al.*, 2000) and between pentamers of LS from *C. albicans* (Morgunova *et al.*, 2007). Although indirect and of low affinity (as judged from our SEC result, Fig. 2), this mode of decamer formation appears to be conserved.

The *C. glabrata* LS monomer consists of 168 amino acids folding into the $\alpha/\beta/\alpha$ sandwich topology common to other LSs. The first ten N-terminal residues of each monomer are disordered, with only that of chain *D* being modelled. The overall structure of the monomeric subunit is very similar to those of LS from both *S. cerevisiae* and *C. albicans*, with some variation in the loop region between α4 and α5 from both the *C. albicans* and the *Schizosaccharomyces pombe* structures (Fig. 5). The sequence of the loop in *C. glabrata* LS appears to be more similar to that of *S. cerevisiae* than to that of *C. albicans*. The α2 helix is extended when compared with the same region in LS from *S. pombe* and the hyperthermophile *Aquifex aeolicus*, in which the latter exists in an icosahedral form (Zhang *et al.*, 2001).

After several rounds of refinement, density was evident in several active sites. Glycerol was initially modelled into these positions; however, additional contiguous density made it clear that there was another molecule present. One molecule of the catalytic product 6,7-dimethyl-8-(D-ribityl)lumazine was modelled into each pentamer (Fig. 6). In a separate crystallization experiment (data not shown), an attempt was made to cocrystallize *C. glabrata* LS with a previously published inhibitor of *S. pombe* and *M. tuberculosis* LS (Talukdar *et al.*, 2009). Refinement of the resulting crystallographic data

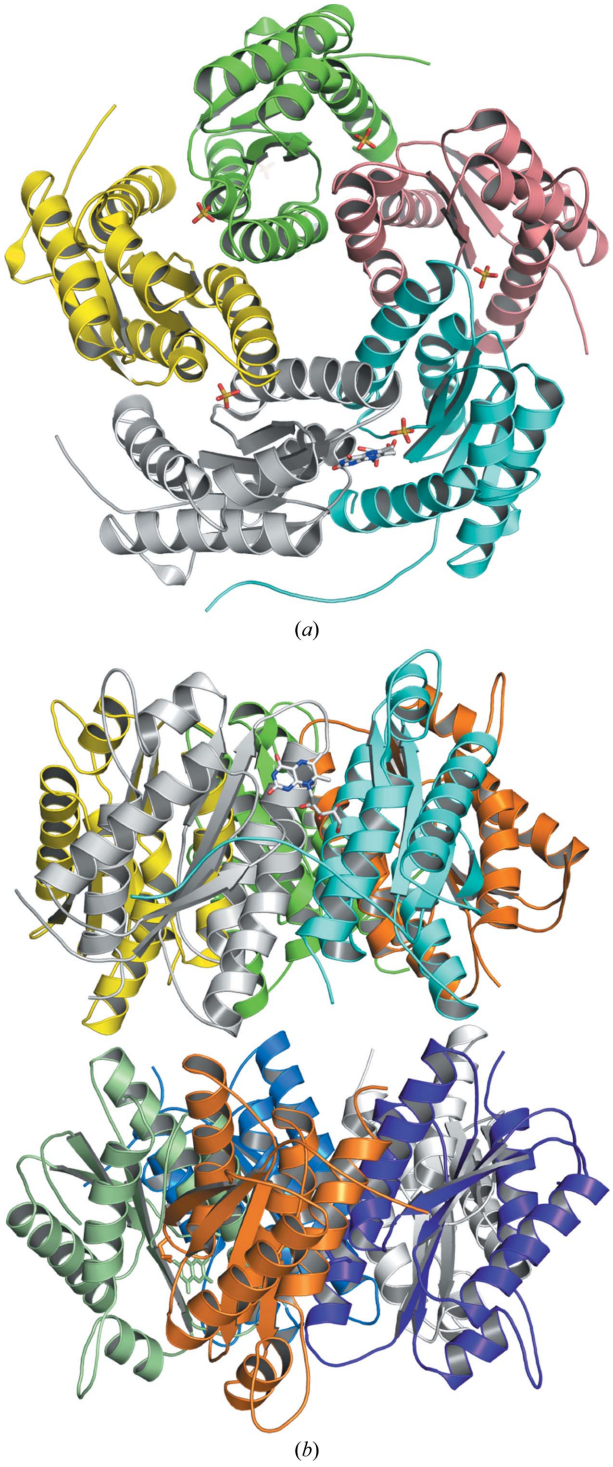

Figure 3
(*a*) Pentameric subunit of *C. glabrata* LS complexed with 6,7-dimethyl-8-(D-ribityl)lumazine viewed along the fivefold axis. (*b*) LS decamer viewed perpendicular to the fivefold axis. Each monomer is shaded in a different colour. Catalytic product and sulfate ions are shown as sticks, with white C atoms, blue N atoms, red O atoms and yellow S atoms.

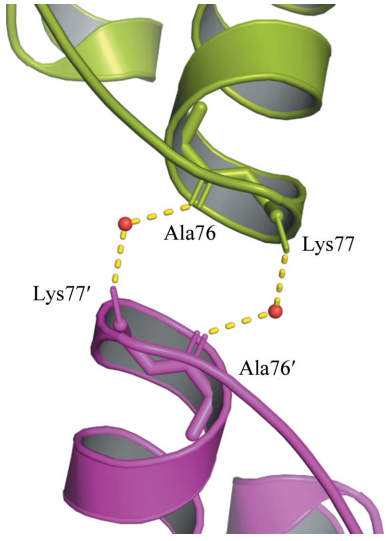

Figure 4
Water-mediated hydrogen bonding between pentameric subunits. The orientation approximates that of the cyan and purple subunits in Fig. 3(*b*). The main-chain atoms of Ala76 and Lys77 are shown to illustrate the hydrogen-bonded interaction.

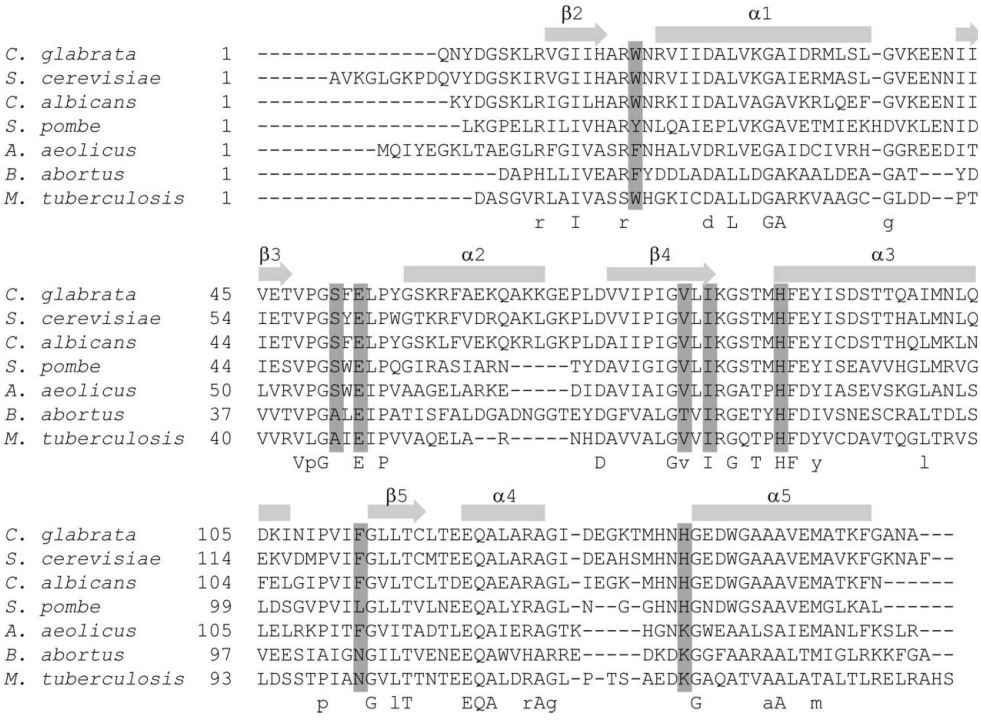

Figure 5
Structure-based sequence alignment of LS from different species. The sequences used are those deposited in the PDB (*S. cerevisiae*, 1ejb; *C. albicans*, 2jfb; *S. pombe*, 2a57; *A. aeolicus*, 1nqu; *B. abortus*, 2i0f; *M. tuberculosis*, 2c92). The alignment was carried out with *MUSTANG* v.3.2.1 (Konagurthu *et al.*, 2006). Key residues within the active site are highlighted and the secondary structure of *C. glabrata* LS is shown above, with cylinders and arrows representing α-helices and β-strands, respectively.

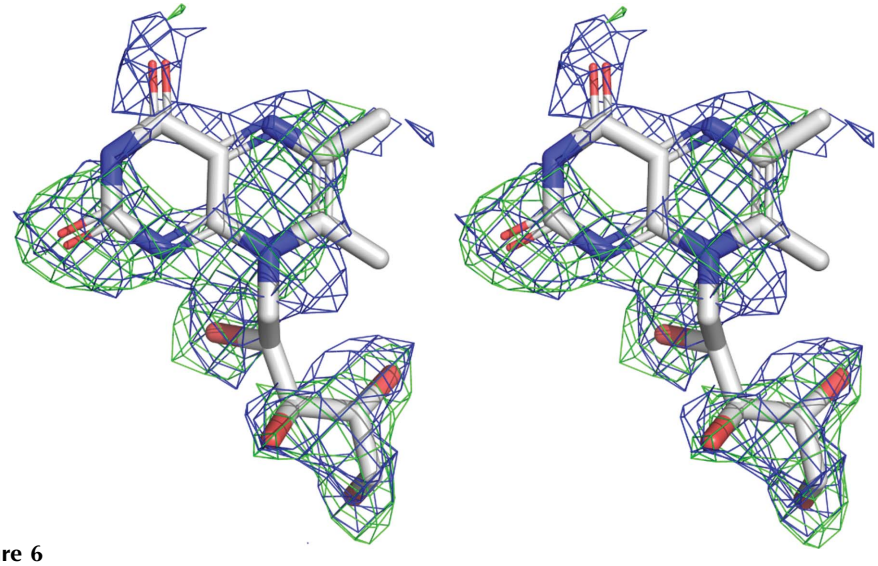

Figure 6
OMIT maps. This stereo diagram shows electron density in the active site, with the final model of 6,7-dimethyl-8-(D-ribityl)lumazine shown as sticks coloured as in Fig. 3. The $2F_o - F_c$ map (blue) is contoured at 1σ and the $F_o - F_c$ map (green) is contoured at 2σ. Both maps were calculated using F_{calc} from coordinates refined with no ligand in the active site.

showed that a product molecule fitted the maps better than the inhibitor (Supplementary Material[1]).

[1] Supplementary material has been deposited in the IUCr electronic archive (Reference: BE5230). Services for accessing this material are described at the back of the journal.

3.3. Ligand identification

Mass spectrometry of the protein solution used for crystallization confirmed the presence of 6,7-dimethyl-8-(D-ribityl)lumazine (Fig. 1; labelled **3**, $C_{13}H_{19}O_6N_4$) with an m/z of 327.1943 (predicted 327.12991). A daughter ion ($C_8H_9O_2N_4$) was also identified which matched the loss of the ribityl chain ($C_5H_{10}O_4$) with an m/z of 193.07204 (predicted 193.07200). Fluorescence spectra were collected from the protein sample and a reference sample of riboflavin. The LS protein sample gave excitation and emission peaks at 410 and 480 nm, respectively, similar to previously published spectra for 6,7-dimethyl-8-(D-ribityl)lumazine (excitation maximum, 407 nm; emission maximum, 491 nm; Koka & Lee, 1979), while riboflavin gave peaks at 445 and 521 nm, respectively (reference excitation, 447 nm; emission, 517 nm; Schulman, 1971). The peaks for the LS protein sample are in good agreement with the published data and suggest that the LS protein sample does not contain riboflavin. Traces of the catalytic product have previously been found in *S. pombe* LS expressed in *E. coli* (Fischer *et al.*, 2002). These data support our mass-spectrometry data for the product complex.

3.4. Active-site binding

Despite the application of noncrystallographic symmetry restraints, electron density for the product 6,7-dimethyl-8-(D-ribityl)-lumazine was observed in only one of the five active sites in each pentamer. The ribityl chain forms extensive hydrogen bonds to the side-chain carboxylate of Glu63, the main-chain N atom of Phe62 and the main-chain N atom and O atom of Phe123′ on the adjacent chain (Fig. 7). These interactions are commonly seen in riboflavin complexes (Gerhardt *et al.*, 2002; Koch *et al.*, 2004) and inhibitor complexes (Meining *et al.*, 2000; Zhang *et al.*, 2008) of LS from other species. The non-aromatic 6,7-dimethyl lumazine ring

system forms a key π-stacking interaction with Trp27 (above the plane of the page, not shown for clarity; compare Fig. 8) and makes hydrogen bonds to the main-chain N atom of Ile92, the main-chain O atom of Val90 and the main-chain N atom and side-chain O atom of Ser61. Three other hydrogen bonds are formed *via* water molecules. Close contacts (<3 Å) exist between the catalytic His98 and the methyl C atoms at positions 6 and 7. The product molecule is in an almost identical position and makes similar polar interactions with the isostructural product mimic crystallized with the *A. aeolicus* LS in which the C6 and C7 methyl groups are replaced by carbonyl groups (Zhang *et al.*, 2001). The major differences are a different orientation of His98 (*C. glabrata* numbering), substitution of Trp27 by a Phe whilst still maintaining the key π-stacking interaction and substitution of His149′ by a disordered Lys. A similar product mimic has also been crystallized with a W27Y mutant of LS from *S. pombe* in which only the C7 methyl group is replaced by a carbonyl group (Koch *et al.*, 2004).

A sulfate molecule (not shown for clarity), which occupies the phosphate-binding site of the substrate DHBP, is present in all active sites and forms a salt bridge with Arg137′ as well as hydrogen bonding to Thr96 and in one monomer to Ser95. In both ligand-bound active sites Gly143″ from a neighbouring pentamer abuts Trp27 (3.3 Å), potentially trapping the product in the active site (Fig. 8). The Gly143″ interaction is only observed in these two active sites, suggesting that crystal contacts contribute to trapping one product molecule per pentamer. Similar crystal packing is also observed in both the *S. cerevisiae* LS–inhibitor complex (Meining *et al.*, 2000) and the unliganded *C. albicans* LS (Morgunova *et al.*, 2007), raising the possibility that this interaction may persist independently of the crystallization conditions and could contribute to the observation of decamers in solution (Fig. 2). In addition, the N-terminus of the adjacent monomer chain is more ordered and lies immediately below this symmetry-related molecule. The unliganded *C. albicans* LS structure has numerous closely packed water molecules in the active site. These occupy positions that are superimposable on the N1 and O2 atoms of the product, suggesting that these maps may also show traces

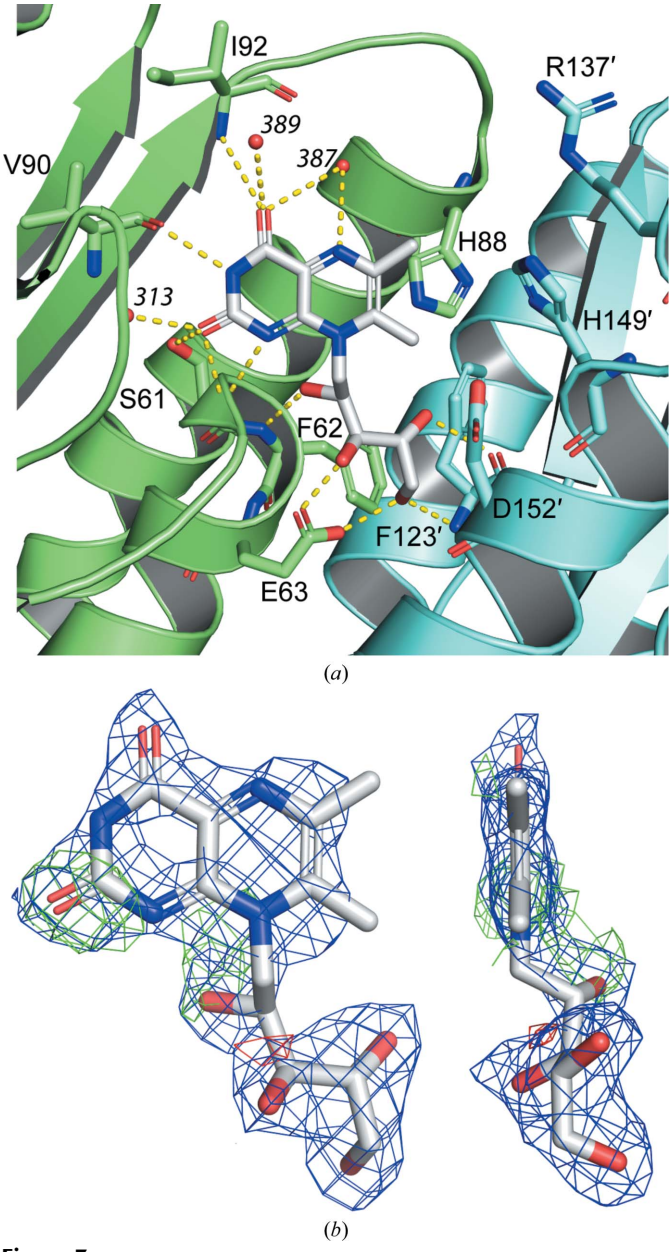

Figure 7
6,7-Dimethyl-8-(D-ribityl)lumazine interactions within the active site. (*a*) Hydrogen bonds are formed between Ile92, Val90, Ser61, Phe62, Glu63 and Phe123′ and the product (**3**). Additional hydrogen bonds are made *via* the conserved water 313 as well as waters 387 and 389. Chain *C* is coloured green, chain *D* is coloured cyan and the product is coloured as in Fig. 3. (*b*) Electron-density maps for the product molecule in chain *C* ($2F_o - F_c$ in blue contoured at 1σ, negative $F_o - F_c$ in red contoured at -3σ, positive $F_o - F_c$ contoured at 3σ within 1.6 Å); the second representation is rotated by 90° and the product is coloured as above. The product molecule is refined with 50% occupancy, except for the glycerol moiety of the ribityl chain, which was refined with 100% occupancy.

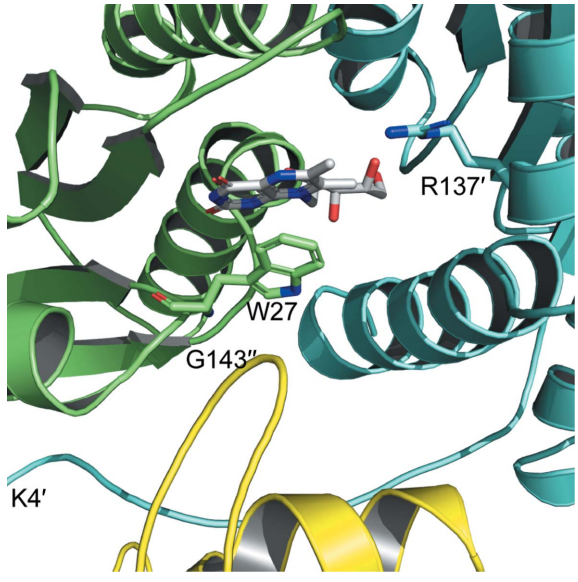

Figure 8
The product molecule is indirectly trapped in the active site by a symmetry-related molecule (yellow) blocking the rotation of Trp27. This view has been rotated forward by ∼90° relative to Fig. 7 around a horizontal axis in the plane of the page.

of product. Others have also shown that LS forms complexes with riboflavin (Fischer *et al.*, 2002; Koch *et al.*, 2004). In some of the active sites where the product is not bound, continuous density similar to that of the ribityl chain could be seen. Glycerol molecules matching the tail of the ribityl chain were built in, as glycerol was used as a cryoprotectant and may have bound at the active site. Outside the crystal contacts, a key interaction between any ligand in the active site is the π-stacking interaction with Trp27. In the eight other sites lacking the product Trp27 appears to be relatively free to rotate and exists in a position perpendicular to that observed in sites with a ligand bound. This orientation precludes binding of the pyrimidinedione or lumazine rings.

4. Future prospects

In this study, we unexpectedly crystallized an LS complex containing the catalytic product 6,7-dimethyl-8-(D-ribityl)-lumazine. This product was previously found to bind to *S. pombe* LS with a K_d of 2 μM (Fischer *et al.*, 2002). As a potential drug target for antifungal agents, LS appears to be promising as it is part of an essential biosynthetic pathway. However, our result suggests that the ability of LS to retain copies of the catalytic product must be considered in the design of inhibitors and in the preparation of LS for inhibitor screening, as inhibitors will need to have a higher binding affinity for the enzyme in order to displace the product.

This work was funded by grants from the Maurice and Phyllis Paykel Trust, the New Zealand Pharmacy Education and Research Foundation (NZPERF) and the New Zealand Dental Association (NZDA). We are grateful to the University of Otago Centre for Protein Research for mass-spectrometric analysis.

References

Battye, T. G. G., Kontogiannis, L., Johnson, O., Powell, H. R. & Leslie, A. G. W. (2011). *Acta Cryst.* D**67**, 271–281.
Chen, S., Slavin, M., Nguyen, Q., Marriott, D., Playford, E. G., Ellis, D. & Sorrell, T. (2006). *Emerg. Infect. Dis.* **12**, 1508–1516.
Emsley, P., Lohkamp, B., Scott, W. G. & Cowtan, K. (2010). *Acta Cryst.* D**66**, 486–501.
Evans, P. (2006). *Acta Cryst.* D**62**, 72–82.
Fischer, M. & Bacher, A. (2008). *Arch. Biochem. Biophys.* **474**, 252–265.
Fischer, M. & Bacher, A. (2011). *Chembiochem*, **12**, 670–680.
Fischer, M., Haase, I., Feicht, R., Richter, G., Gerhardt, S., Changeux, J.-P., Huber, R. & Bacher, A. (2002). *Eur. J. Biochem.* **269**, 519–526.
Gerhardt, S., Haase, I., Steinbacher, S., Kaiser, J. T., Cushman, M., Bacher, A., Huber, R. & Fischer, M. (2002). *J. Mol. Biol.* **318**, 1317–1329.
Kis, K., Volk, R. & Bacher, A. (1995). *Biochemistry*, **34**, 2883–2892.
Klinke, S., Zylberman, V., Vega, D. R., Guimarães, B. G., Braden, B. C. & Goldbaum, F. A. (2005). *J. Mol. Biol.* **353**, 124–137.
Koch, M., Breithaupt, C., Gerhardt Haase, S., Weber, S., Cushman, M., Huber, R., Bacher, A. & Fischer, M. (2004). *Eur. J. Biochem.* **271**, 3208–3214.
Koka, P. & Lee, J. (1979). *Proc. Natl Acad. Sci. USA*, **76**, 3068–3072.
Konagurthu, A. S., Whisstock, J. C., Stuckey, P. J. & Lesk, A. M. (2006). *Proteins*, **64**, 559–574.
Krissinel, E. & Henrick, K. (2007). *J. Mol. Biol.* **372**, 774–797.
Kumar, P., Singh, M. & Karthikeyan, S. (2011). *Acta Cryst.* D**67**, 131–139.
Kusne, S. & Blair, J. E. (2006). *Liver Transpl.* **12**, 2–11.
Malani, A., Hmoud, J., Chiu, L., Carver, P. L., Bielaczyc, A. & Kauffman, C. A. (2005). *Clin. Infect. Dis.* **41**, 975–981.
Massey, V. (2000). *Biochem. Soc. Trans.* **28**, 283–296.
Meining, W., Mörtl, S., Fischer, M., Cushman, M., Bacher, A. & Ladenstein, R. (2000). *J. Mol. Biol.* **299**, 181–197.
Messer, S. A., Jones, R. N. & Fritsche, T. R. (2006). *J. Clin. Microbiol.* **44**, 1782–1787.
Morgunova, E., Illarionov, B., Saller, S., Popov, A., Sambaiah, T., Bacher, A., Cushman, M., Fischer, M. & Ladenstein, R. (2010). *Acta Cryst.* D**66**, 1001–1011.
Morgunova, E., Meining, W., Illarionov, B., Haase, I., Jin, G., Bacher, A., Cushman, M., Fischer, M. & Ladenstein, R. (2005). *Biochemistry*, **44**, 2746–2758.
Morgunova, E., Saller, S., Haase, I., Cushman, M., Bacher, A., Fischer, M. & Ladenstein, R. (2007). *J. Biol. Chem.* **282**, 17231–17241.
Murshudov, G. N., Skubák, P., Lebedev, A. A., Pannu, N. S., Steiner, R. A., Nicholls, R. A., Winn, M. D., Long, F. & Vagin, A. A. (2011). *Acta Cryst.* D**67**, 355–367.
Pfaller, M. A. & Diekema, D. J. (2007). *Clin. Microbiol. Rev.* **20**, 133–163.
Pfaller, M. A. & Diekema, D. J. (2010). *Crit. Rev. Microbiol.* **36**, 1–53.
Pfaller, M. A., Diekema, D. J. & Sheehan, D. J. (2006). *Clin. Microbiol. Rev.* **19**, 435–447.
Rajeshkumar, R. & Sundararaman, M. (2012). *Mycoses*, **55**, e60–e73.
Schulman, S. G. (1971). *J. Pharm. Sci.* **60**, 628–631.
Talukdar, A., Breen, M., Bacher, A., Illarionov, B., Fischer, M., Georg, G., Ye, Q.-Z. & Cushman, M. (2009). *J. Org. Chem.* **74**, 5123–5134.
Winn, M. D. *et al.* (2011). *Acta Cryst.* D**67**, 235–242.
Zhang, Y., Illarionov, B., Morgunova, E., Jin, G., Bacher, A., Fischer, M., Ladenstein, R. & Cushman, M. (2008). *J. Org. Chem.* **73**, 2715–2724.
Zhang, X., Meining, W., Fischer, M., Bacher, A. & Ladenstein, R. (2001). *J. Mol. Biol.* **306**, 1099–1114.